Journal of Minerals and Materials Characterization and Engineering, 2023, 11, 161-171
https://www.scirp.org/journal/jmmce
ISSN Online: 2327-4085
ISSN Print: 2327-4077

Hydrogen Embrittlement of Nitrogenating Layer on Martensitic Alloys

Daniel Moreno, Yohanan Nachmana, Shimon Bashan, Barak Weizman, Denis Panchenko, Michael Mansano, Elinor Itzhak, Moshe Shapira

Beth Shemesh Engines Ltd., FAA&EASA, Beth Shemesh, Israel

Email: danielm@bsel.co.il

How to cite this paper: Moreno, D., Nachmana, Y., Bashan, S., Weizman, B., Panchenko, D., Mansano, M., Itzhak, El. and Shapira, M. (2023) Hydrogen Embrittlement of Nitrogenating Layer on Martensitic Alloys. *Journal of Minerals and Materials Characterization and Engineering*, **11**, 161-171.
https://doi.org/10.4236/jmmce.2023.115013

Received: July 18, 2023
Accepted: September 5, 2023
Published: September 8, 2023

Abstract

Nitriding of the surface in martensitic stainless steels is commonly carried out to improve their wear resistance. The process of plasma nitriding in stainless steel is influenced by two mechanisms: physical diffusion through the surface and chemical gas-metal reaction. The inner nitriding interaction involves the simultaneous penetration and formation of a solid solution, as well as the interaction of nitrogen with specific alloying elements, resulting in the development of homogeneous and heterogeneous structures. Our study concludes that the observed intergranular hydrogen embrittlement and crack formation during the surface nitridation process of AMS 5719 martensite alloy steel can be attributed to the ammonium concentration of approximately 50% at a temperature of 530˚C.

Keywords

Hydrogen Embrittlement, Nitriding Coat, Cracks, Martensite Steel, Surface Hardness

1. Introduction

The mechanical properties of AMS 5719, a chromium martensitic stainless steel, are attributed to its double tempering heat treatment, which results in high-temperature strength, excellent creep resistance, corrosion resistance, very good toughness, and temper resistance at temperatures up to 560˚C. The chemical composition of AMS 5719 is characterized as a Cr-Mo martensitic alloy and is primarily used in aerospace manufacturing for turbine blades, turbine discs, and other parts designed for high heat and high-stress environments. Nitriding of the surface in martensitic stainless steels is performed to enhance wear resistance. Common techniques for nitriding the surface include conventional gas

nitriding, ion nitriding, and liquid salt bath nitriding [1] [2] [3] [4]. Most stainless-steel alloys exhibit a three-layer structure during nitridation, which can be observed under optical magnification. The layers consist of the subsurface, typically composed of the ε phase, the second layer comprised of metastable phases (γ-N) and expanded martensite (α-N) with precipitates of MN-type nitrides (often CrN), and the deeper zone adjacent to the steel core enriched with carbon [5] [6]. Two mechanisms are considered for simultaneous penetration and the formation of a solid solution or interaction of nitrogen in the metal structure: physical diffusion and chemical gas-metal reaction. The activation of nitrogen atoms on the metal surface depends on the atmosphere used and its concentration. For example, the addition of oxygen, air, and carbon dioxide increases the rate of nitrogen diffusion saturation in steel [7]. This increase in saturation is attributed to the decrease in the partial pressure of NH_3 in the heterogeneous atmosphere due to the binding of free hydrogen, as described by the reaction $H_2 + 1/2\ O_2 \rightarrow H_2O$. The heterogeneous atmosphere is defined as containing NO, H_2, H_2O, N_2, and ammonia NH_3, and its composition depends greatly on the process temperature. The surface hardness of nitride austenitic and martensitic stainless steels increases significantly, but it varies depending on the process. In the case of nitride austenitic stainless steel, hardening occurs at low temperatures and is attributed to the formation of fine γ-Fe_4N and CrN precipitates in the matrix. At higher temperatures, precipitation hardening is responsible for the increased hardness. Martensitic stainless-steel exhibits a different hardening mechanism attributed to the Fe_2 + xN phases [8]. In the plasma nitriding of AISI 420 martensitic stainless steel, the process at lower temperatures is governed by diffusion through the surface, while the inner nitriding process is governed by homogeneous and heterogeneous processes. The homogeneous process, involving nitrogen supersaturation, leads to a phase transformation from α'- to γ-phase and plastic straining, resulting in recrystallization of small grains driven by nitrogen intergranular diffusion. The concentration of nitrogen near the metal front in the process is governed by heterogeneously formed nitrides. The original coarse grains facilitate heterogeneous nitriding under elastic and plastic straining, forming homogeneous nitriding [9]. XRD analysis was conducted to identify the ε and γ' nitride phases after plasma nitriding of a low alloy steel. The increase in hardness was attributed to these phases, which induce stress on the surface [10]. The diffusion coefficient of nitrogen in low alloy steels was found to be 2.23×10^{-13} m^2/s, which is faster than in alloyed steels and conventional nitriding [10]. This change in diffusion kinetics can be attributed to internal stresses between the grains and the formation of new nitrogen reaction phases. During the nitridation process, ammonia (NH_3) dissociates into nitrogen (N_2) and hydrogen (H_2) according to the reaction: $2NH_3 \rightarrow N_2 + 3H_2$. The hydrogen generated in this reaction has the potential to diffuse into the metal, primarily through grain boundaries. It can then recombine with the basic elements present in the steel and form hydrides. The steel microstructure contains various metallurgical fea-

tures, such as dislocations, precipitates, inclusions, and twins, which can act as traps for the small hydrogen atoms. The diffusivity of hydrogen in the ferrite and austenite phases was reported to be $D\alpha \approx 1.5 \times 10^{-11}$ m^2/s and $D\gamma \approx 1.4 \times 10^{-16}$ m^2/s, respectively [11]. The presence of hydrogen in the steel induces stresses and macrostrain, leading to the phenomenon known as Hydrogen Embrittlement (HE) [12]. This can result in the formation and propagation of microcracks, which are attributed to the tearing modulus. A study compared the performance of Ti-Mo alloyed steels with V-Mo alloyed steels in terms of their potential to trap hydrogen [13]. Quantitative metallography analysis indicated that Ti-Mo alloyed steels showed fewer potential traps than V-Mo alloyed steels. It was also observed that twins, which form in the habit planes of the martensitic structure, induce dislocations and local strain [14]. Number of processes were carried out by Saeed *et al.* [15]. The researchers conducted several processes in a gas atmosphere with varying ammonia contents in the temperature range of 425˚C - 475˚C. They performed XRD analysis of nitriding Stainless Steel 304 samples under optimized plasma chamber conditions, using optical emission spectroscopy. The analysis revealed the formation of iron and chromium nitrides, which occurred at a gas composition of 40% H2 in nitrogen plasma. The study concluded that to obtain a good nitriding layer without nitride precipitation, the process should be carried out with an atmosphere containing lower ammonia concentrations than 50% and at temperatures below 450˚C [16].

The inspection of embrittlement and crack formation on the surface nitridation process of an AMS 5719 martensite alloy steel was presented in this work. The discontinuity of the upper layer by intergranular cracks could be attributed to hydrogen embrittlement. The study also includes a similar process conducted on Alloy 431 as a reference, with the findings reported in the research.

2. Experimental

The AMS 5719 chromium martensitic stainless steel alloyed and Alloy 431 (UNS S43100) most corrosion resistant of the martensitic steels with composition [weight %] presented in **Table 1**, were heat treated according to the follow heat treatments:

AMS 5719—Annealing at 691˚C for six hours and air cooled to room temperature. Hardening 1052˚C for 30 minutes, followed by oil quenching. First tempering at 560˚C - 590˚C for one hour, followed by air cooling. Second

Table 1. Alloy composition.

Alloy \ Element	Cr	Mo	Ni	V	Mn	Si	Cu	C	Fe	Traces
AMS 5719	11 - 12.5	1.5 - 2	2 - 3	0.25 - 0.4	0.4 - 0.9	<0.5		0.08 - 0.15	Bal.	Less than 0.5, 0.025, 0.015 and 0.04, P, S and N, respectively
Alloy 431	15.5 - 16.5	0.25	2 - 3	-	0.3	0.2 - 0.6	0.5	0.12 - 0.17	Bal.	Less than 0.1 and 0.04 N and P, respectively.

tempering at 538˚C - 560˚C for three hours, followed by air cooling to room temperature.

Alloy 431—Initially transformed into its austenitic state at 980˚C - 1065˚C for a half hour, quenched and tempered at 690˚C for 8 hr.

Two different nitriding processes were applied to two different alloys: AMS 5719 and Alloy 431.

Process (1)—AMS 5719:

1) Surface Activation: The surface of the AMS 5719 alloy was activated by alumina sputtering (shotting).

2) Nitriding: The activated surface was then subjected to gas nitriding using a nitriding process with an estimated 50% dissociation of ammonia.

3) Temperature and Duration: The nitriding process was carried out at 530˚C for a duration of 60 hours.

Process (2)—Alloy 431:

1) Ammonia Furnace: The Alloy 431 was initially treated in an ammonia furnace for a period of 4 hours.

2) Gas Nitriding: After the ammonia furnace treatment, the surface of Alloy 431 underwent gas nitriding.

3) Graded Nitriding: The gas nitriding process involved a graded increase in the estimated dissociation of ammonia. The dissociation increased from 20% to 50%.

4) Temperature and Duration: Along with the increasing dissociation of ammonia, the temperature was also gradually increased from an initial value up to 560˚C. The gas nitriding process lasted for 48 hours.

5) Carbon Addition: Carbon was added to the atmosphere during the process as a means of hydrogen trapping.

The samples were inspected under optical microscopy to characterize the cross section of the nitride layers follow by micro-hardness in the first level of inspection. Furthermore, the layers were inspected for chemical analyzed under SEM-EDS techniques.

3. Results

The exposed cross section of the nitriding processes is shown in Figure 1(a) & Figure 1(b), for the AMS 5719 alloy and Alloy 431 that were exposed to process (1) and process (2), respectively. Four zones are distinguished in both processes very clear that include a very thin layer on the top (I) characterized as a very saturated by nitrides, second zone from the top (II) as a homogenous nitride zone, third zone from the top (III) as a metastable diffusion nitriding front to the base metal and finally the basic metal (IV). On the AMS 5719 alloy surface the intergranular crack presented in higher magnification in Figure 2, are attributed to the process conditions. The cracks propagate near the surface in zone II, where lower bulk mechanical resistant govern but that mean that all zone III under residual stresses. Moreover, the interface between zone II to zone III shows a discontinuity presented as a parallel crack with the surface, called delamination as

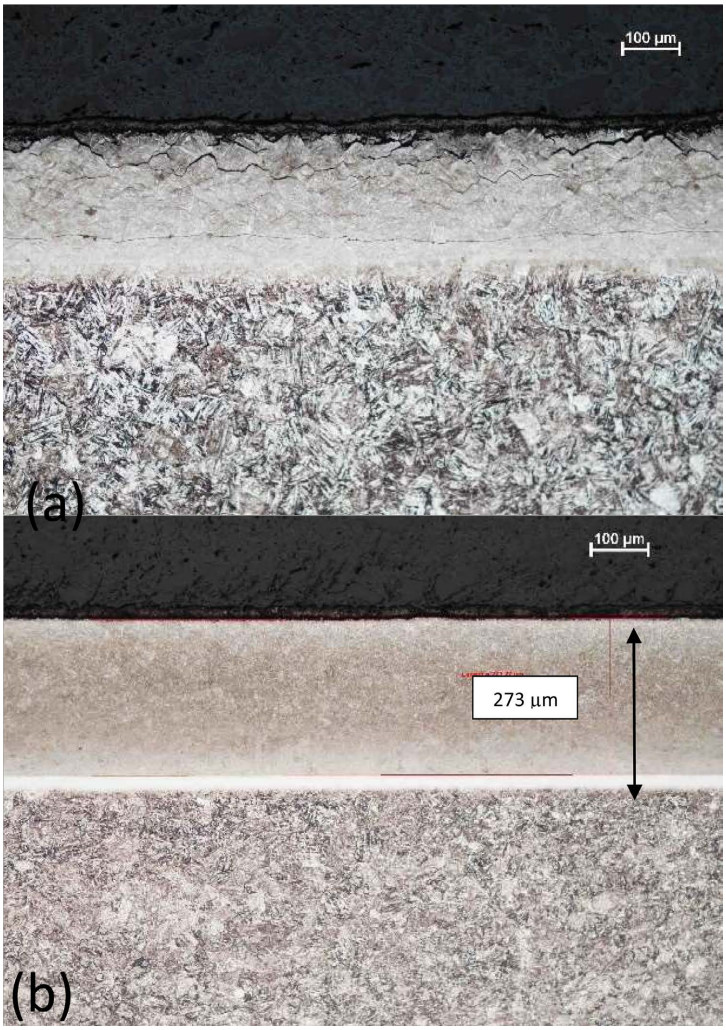

Figure 1. AMS 5719 and Alloy 431 cross-section after nitriding carried out under process (1) in (a) and process (2) in (b), respectively.

show in **Figure 2**. In the other hand, Alloy 431 in **Figure 1(b)**, where the gas nitriding of the surface was carried out in a graded increasing of estimated dissociation of ammonia starting from 20% up to 50%, with parallel increasing of the temperature up to 560˚ during 48 hr., the layer present similar zones from the top but no cracks were observed. Micro-hardness results on the different zones summarized in **Table 2** and visualized in **Figure 3**.

The microhardness shows an obvious behavior and the increasing of the hardness on the surface as excepted. The comparison between both metals shown higher hardness on AMS 5719 and the conclusions are not straightforward. It is difficult to decide if the increasing hardness on Alloy 431 is only by the nitriding process or by the mutual effect of the nitriding and the hydrogen induced in the layer. SEM observation and EDS analysis show in **Figure 4** and **Figure 5** show increase of the Cr and Mo in AMS 5719 alloy and Cr in ASTM 431 with good correlation with the Nitrogen along deep. The decreases of the iron composition are practically only relative to the increase of the Cr, Mo and N.

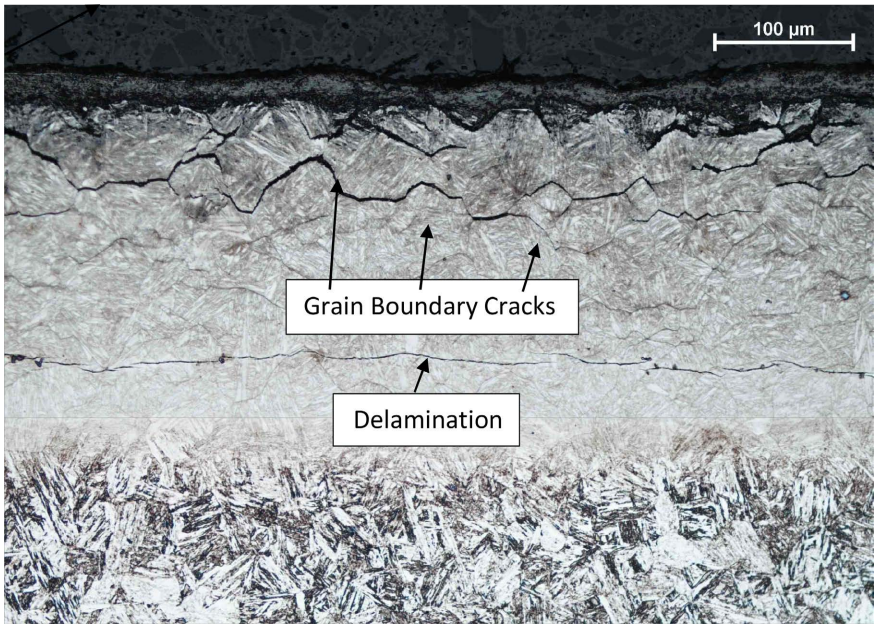

Figure 2. Grain boundaries cracking developed during nitriding process with 50% estimated dissociation of ammonia at 530°C for 60 hrs. Lamination of the layer near the interface between the layer and the basic metal structure.

Table 2. Micro-Hardness in Vickers (HV 0.5 Kg.) at the different zones of the samples.

Sample/Zone	Second zone from the top (II)	Third zone from the top (III)	Basic metal (IV).
AMS5719 (1)	1154, 1118, 1217 avg. - 1163	968, 783, 875 avg. - 875	346, 341, 349 avg. - 345
Alloy 431 (2)	824, 786, 797 avg. - 802	358, 582, 429 avg. - 456	287, 296, 294 avg. - 292

The very thin layer on the top (I) is too thin to perform the test.

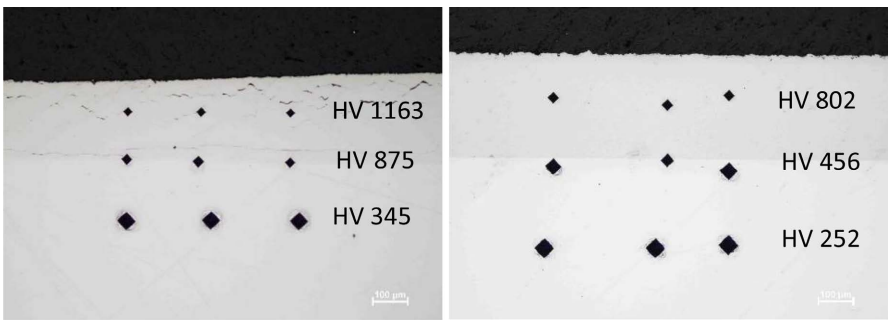

Figure 3. Indentations and Vickers average values of AMS 5719 (a) and ASTM431 (b).

4. Discussion

As reported elsewhere [16], the hydrogen diffusivity is in a large range of two to three orders of magnitude among chromium steel, duplex stainless steels, and austenite stainless steels 300 series. Trap occupancy as vacancies, dislocations, grain boundaries, inclusions, precipitates in metals effects on the hydrogen

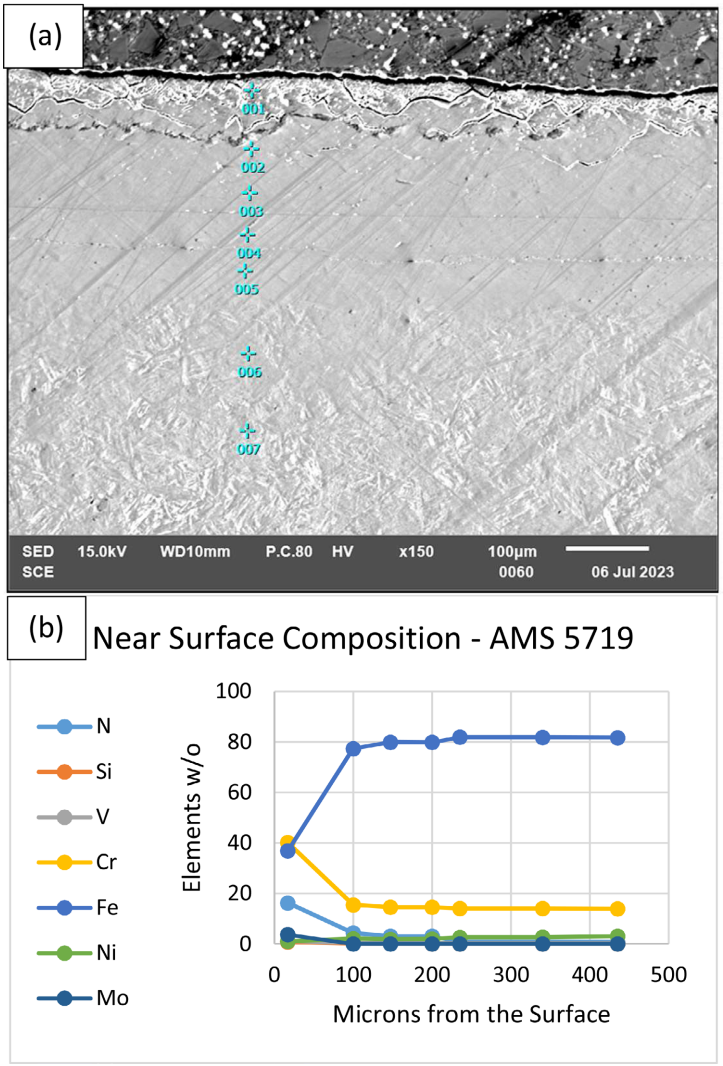

Figure 4. Cross section image of the EDS analyzed points in the AMS 5719 sample after process (1) in (a), and elements composition from the surface (b). Iron composition drop near the surface when Cr, Mo and N increase, leading to the assumption that Cr_xN_y and Mo_xN_y nitriding are recombine.

diffusivity [17] [18]. Moreover, the effective diffusivity of hydrogen AISI 410 steel is almost 2 time higher than the effective diffusivity in a Cr steel, attributed to the austenite phase content. Martensite alloys as AISI 410 with a very low retained austenite, the absorption of hydrogen trapping is mainly by the association of the hydrogen with carbides inclusions [16]. Hydrogen embrittlement mechanism reported include Adsorption Induced Dislocation Emission (AIDE), Hydrogen Enhanced Localized Plasticity (HELP), and Hydrogen Enhanced Decohesion Embrittlement (HEDE) all based on the hydrogen diffuses into the metal in weakens interatomic bond. Atomistic simulations in BCC iron metals shows two symmetric sinks to interstitial hydrogen atom in the lattice: octahedral site and a tetrahedral site with a large volume with an isotopic stress field that attract hydrogen adsorption [16]. In this report, AMS 5719 chromium

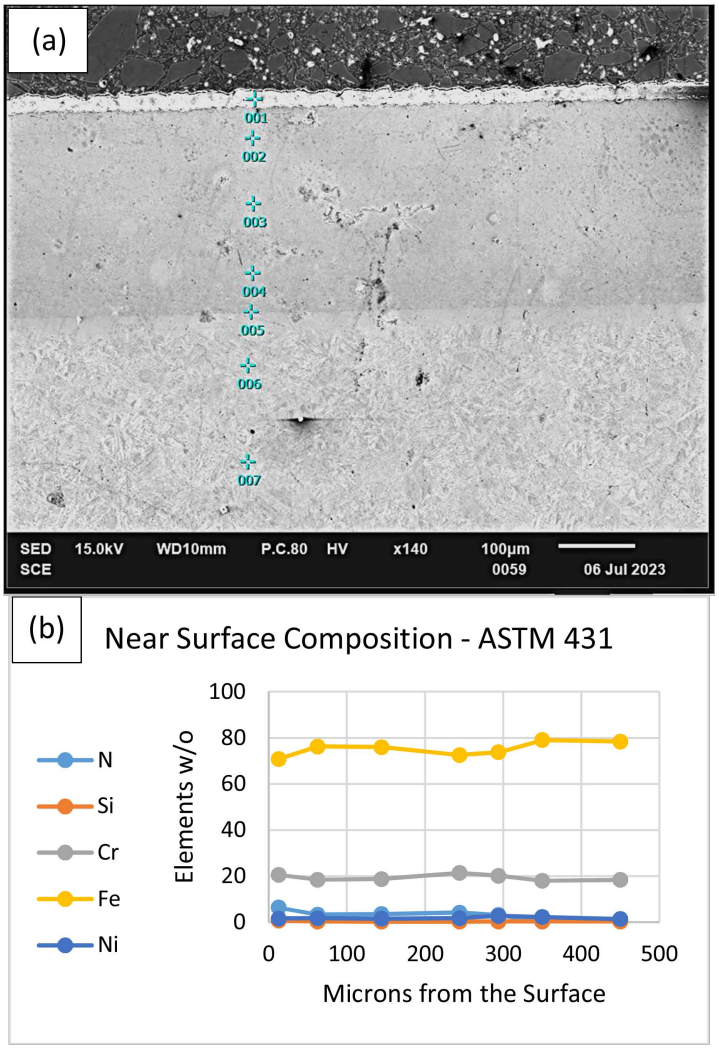

Figure 5. Cross section image of the EDS analyzed points in the ASTM 431 sample after process (2) in (a), and elements composition from the surface (b). Small decrease of Iron composition near the surface when Cr and N increase, leading to the assumption that Cr_xN_y nitriding are recombine but good homogeneity was observed.

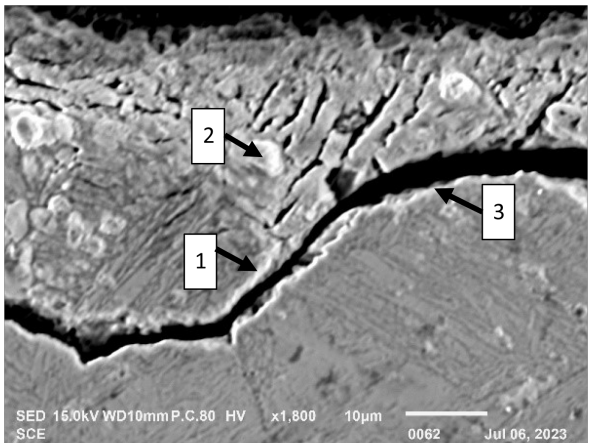

Figure 6. EDS analysis in the crack zone of sample AMS 5719 (zone 1) shows Nitrogen/Chromium relation of 1/4, 1/2 and 2/5 at points 1, 2 and 3, respectively.

martensitic stainless steel that carbon atoms form chromium-carbide phases dispersed mainly in the grain boundaries use as diffusion sinks and hydrogen traps. This adsorption weak the grain boundaries leading to cracks and stress the crystal lattice leading to stresses and depends very much on the hydrogen concentration in the atmosphere environment, process temperature and the metallurgical structure of the metal. One of the mainly difference between both nitrating processes is the ammonia concentration. The dissociation of the ammonia molecule according to $2NH_3 \Rightarrow N_2 + 3H_2$ shows that 75% of the dissociation form pure hydrogen. Most of the hydrogen recombine with the added carbon in process (2) forming methane (CH_4) and avoid the hydrogen to induce in high concentration to diffuse to the nitride layer. Rather than in process (1) that is characterized with higher temperature, higher ammonia concentration and without carbon gather to significantly reduce the amount of hydrogen when the N diffuse to the metal. The cracks observed in the AMS 5719 where process (1) was used are attributed to the large amount of hydrogen at high temperature during 60 hr. and the very good layer obtained in Alloy 431 where process (2) was carried out is attributed to the very low level of free hydrogen in the atmosphere although with some amount of methane, and the graded increasing of the ammonia concentration and the temperature. The nitriding process in alloy ASTM 321 precented in **Figure 5(a)** & **Figure 5(b)** shows good homogeneity of the elements along the deep of the layer and is attributed to the continues diffusion of the elements during nitriding process. The nitriding process in AMS 5719 alloy shows very different behavior. The intergranular cracks attributed to the high concentration of hydrogen in the atmosphere environment by hydrogen embrittlement create a discontinuity between the deeper zones. This discontinuity pills up the nitride and chromium in the 100 microns near the surface as shown in **Figure 4(a)** & **Figure 4(b)**, that lead to concentrate brittle phases in the grain boundaries to be attacked by hydrogen and forming intergranular cracks. **Figure 6** presents the enhancement of the crack zone and EDS analysis of phases found in the image to revel the Nitrogen/Chromium relation of 1/4, 1/2 and 2/5 at points 1, 2 and 3 in a, respectively. Molybdenum-hydride could be existing under high external pressure of 6 GPa and temperatures up to 800˚C [13] and is not clear the small increase of Molybdenum to the surface. Also, Vanadium-Hydride is very rare in metals and Cu does not for hydrides and mainly produced as a reducing agent in organic synthesis. We assume that the chemical composition could affect in the diffusion rates but do not affect the creation of cracks. The optical and electron microscopy with addition to the EDS cross-section analysis are consistent with even though hydrogen contain is not detected by EDS as a light element and limitation of the technique. Micro-hardness was added as additional information as part of the characterization of the layer properties and show increasing in the hardness in both metals as expected. Is not clear if the additional hardness obtained in the AMS 5719 is or not the effect of the nitriding with the induced hydrogen or not but the brittleness of the layer can be ex-

plained by the hydrogen contain that lead to cracks and micro-cracks rather than in Alloy 431, both martensitic alloys. Martensite needles can be observed in the layer zone that contribute to the unstable phase and minimalize the local strain to fracture range as a brittle and potential zone to cracks. As explained elsewhere by Gong *et al.* [14], the formation of twins attributed to hydrogen induces dislocation mobility and dense dislocation tangles enhance sinks in the nanostructure leading to cracks by hydrogen embrittlement.

5. Conclusion

In this study, we examined the nitriding cross-section layers of two martensitic alloys, namely AMS 5719 and Alloy 431, using optical and electron microscopies, along with EDS analysis and micro-hardness testing. Our investigation focused on understanding the phenomena of embrittlement and crack formation observed during the surface nitridation process of AMS 5719 martensite alloy steel, specifically attributing it to an approximate ammonium concentration of 50% at 530˚C. We determined that the discontinuity observed in the upper layer is a result of intergranular hydrogen embrittlement caused by the dissociation of ammonia as described by the reaction $2NH_3 \rightarrow N_2 + 3H_2$. Additionally, we conducted a similar process on Alloy 431 as a reference material, and the findings from this comparative analysis are also presented in this research.

Conflicts of Interest

The authors declare no conflicts of interest regarding the publication of this paper.

References

[1] Shen, Y.Z., Oh, K.H. and Lee, D.N. (2005) Nitriding of Steel in Potassium Nitrate Salt Bath. *Scripta Materialia*, **53**, 1345-1349. https://doi.org/10.1016/j.scriptamat.2005.08.032

[2] Tsujimura, H., Goto, T. and Ito, Y. (2004) Electrochemical Surface Nitriding of Pure Iron by Molten Salt Electrochemical Process. *Journal of Alloys and Compounds*, **376**, 246-250. https://doi.org/10.1016/j.jallcom.2003.12.042

[3] Li, H.Y., Luo, D.F., Yeung, C.F. and Lau, K.H. (1997) Microstructural Studies of QPQ Complex Salt Bath Heat-Treated Steels. *Journal of Materials Processing Technology*, **69**, 45-49. https://doi.org/10.1016/S0924-0136(96)00037-4

[4] Yeung, C.F., Lau, K.H., Li, H.Y. and Luo, D.F. (1997) Advanced QPC Complex Salt Bath Heat Treatment. *Journal of Materials Processing Technology*, **66**, 249-252. https://doi.org/10.1016/S0924-0136(96)02535-6

[5] Kochmanski, P., Długozima, M. and Baranowska, J. (2022) Structure and Properties of Gas-Nitrided, Precipitation-Hardened Martensitic Stainless Steel. *Materials*, **15**, Article 907. https://doi.org/10.3390/ma15030907

[6] Zinchenko, V.M., Syropyatov, V.Y., Barelko, V.V. and Bykov, L.A. (1997) Gas Nitriding in Catalytically Prepared Ammonia Media. *Metal Science and Heat Treatment*, **39**, 280-284. https://doi.org/10.1007/BF02467122

[7] Zinchenko, V.M. and Georgievskaya, B.V. (1983) Nitrocarburization of Automobile

Parts. NII Tavtoprom, Moscow. (In Russian)

[8] Lin, Y.H., Wang, J., Zeng, D.Z., Huang, R.B. and Fan, H.Y. (2013) Advance Complex Liquid Nitriding of Stainless Steel AISI 321 Surface at 430C. *Journal of Materials Engineering and Performance JMEPEG/ASM International*, **22**, 2567-2573. https://link.springer.com/article/10.1007/s11665-013-0545-8

[9] Aizawa, T., Yoshino, T., Morikawa, K. and Yoshihara, S.I. (2019) Microstructure of Plasma Nitrided AISI420 Martensitic Stainless Steel at 673 K. *Crystals*, **9**, Article 60. https://www.mdpi.com/journal/crystals

[10] Mohan Rao, K.R., Trinadh, K. and Nouveau, C. (2019) Glow Discharge Plasma Nitriding of Low Alloy Steel. *Materials Today*: *Proceedings*, **19**, 864-866. https://doi.org/10.1016/j.matpr.2019.08.224

[11] Owczarek, E. and Zakroczymski, T. (2000) Hydrogen Transport in a Duplex Stainless Steel. *Acta Materialia*, **48**, 3059-3070. https://doi.org/10.1016/S1359-6454(00)00122-1

[12] Nagao, A., Smith, C.D., Dadfarnia, M., Sofronis, P. and Robertson, I.M. (2012) The Role of Hydrogen in Hydrogen Embrittlement Fracture of Lath Martensitic Steel. *Acta Materialia*, **60**, 5182-5189. https://doi.org/10.1016/j.actamat.2012.06.040

[13] Kuzovnikov, M.A., Meng, H. and Tkacz, M. (2017) Nonstoichiometric Molybdenum Hydride. *Journal of Alloys and Compounds*, **694**, 51-54. https://doi.org/10.1016/j.jallcom.2016.09.288

[14] Gong, P., Nutter, J., Rivera-Diaz-Del-Castillo, P.E.J. and Rainforth, W.M. (2020) Hydrogen Embrittlement through the Formation of Low-Energy Dislocation Nanostructures in Nanoprecipitation-Strengthened Steels. *Science Advances*, **6**, eabb6152. https://doi.org/10.1126/sciadv.abb6152

[15] Saeed, A., Khan, A.W., Jan, F., SHhah, H.U., Abrar, M., Zaka-Ul-Islam, M., Khalid, M. and Zakaullah, M. (2014) Optimization Study of Pulsed DC Nitrogen-Hydrogen Plasma in the Presence of an Active Screen Cage. *Plasma Science and Technology*, **16**, 460-464. https://doi.org/10.1088/1009-0630/16/5/04

[16] Hinds, G., Zhao, J., Griffiths, A.J. and Turnbull, A. (2005) Hydrogen Diffusion in Super 13% Chromium Martensitic Stainless Steel. *Corrosion*, **61**, 348-354. https://www.researchgate.net/publication/240846169

[17] Barrera, O., Bombac, D., Chen, Y., Daff, T.D., Galindo-Nava, E., Gong, P., Haley, D., Horton, R., Katzarov, I., Kermode, J.R., Liverani, C., Stopher, M. and Sweeney, F. (2018) Understanding and Mitigating Hydrogen Embrittlement of Steels: A Review of Experimental, Modelling and Design Progress from Atomistic to Continuum. *Journal of Materials Science*, **53**, 6251-6290. https://doi.org/10.1007/s10853-017-1978-5

[18] Kato, H., Hirokawa, W., Todaka, Y. and Yasunaga, K. (2021) Improvement in Surface Roughness and Hardness for Carbon Steel by Slide Burnishing Process. *Materials Sciences and Applications*, **12**, 171-181. http://www.scirp.org/journal/Paperabs.aspx?PaperID=108947